CPFD Simulations on a Chlorination Fluidized Bed Reactor for Aluminum Production: An Optimization Study

Zahir Barahmand[1] Chameera Jayarathna[2] Chandana Ratnayake[1,2]

[1] Department of Process, Energy and Environmental Technology, University of South-Eastern Norway
zbarahmand@gmail.com
[2] SINTEF Tel-Tek, SINTEF Industry, Porsgrunn, Norway

Abstract

Early CPFD simulation studies on designing a fluidized bed reactor for alumina chlorination showed that the model suffers from high particle outflow and dense phase bed channeling. The present study is aimed to optimize the previous alumina chlorination fluidized bed reactor model through modified geometry, parameter modifications, and improved meshing. To optimize the performance of the reactor, complex geometry with an extended top section was combined with a regular cylindrical reactor. Besides, the gas inlet pattern was changed from an ideal uniform distribution to a non-uniform one. Besides, the reactor's inlet diameter is reduced, and the value for the particle sphericity and voidage has been updated based on experimental observations. The results show that the new reactor with an extended cross-sectional area on top has a significantly lower particle outflow even with the higher inlet superficial gas velocity. The paper discusses the optimization steps and relevant changes in reactor performances in detail.

Keywords: Optimization, fluidized bed reactor (FBR), alumina chlorination, Barracuda, CPFD simulation

1 Introduction

Aluminum is now the world's second most used metal (Donaldson & Raahauge, 2013). Since aluminum has a unique combination of appealing properties and functionalities, it allows significant energy savings in many applications, such as vehicles and buildings. Although this energy-saving leads to lower CO_2 emissions, the production process of aluminum still dramatically impacts the environment.

In 1889, the melted cryolite-alumina electrolysis process known as Hall-Héroult (H-H) was started, and the commercial production of metallic aluminum started, and this process has been used almost exclusively in the aluminum production industry (Prasad, 2000). This process has been independently developed and patented, after two young men, oceans apart, around 140 years ago in the United States and France. This discovery in 1886 by C. Hall and P. Héroult has provided the world with the gleaming light metal at reasonable prices. In this method, solid alumina (Al_2O_3) is dissolved in an electrolyte predominantly composed of liquid cryolite (Na_3AlFe_6). The electrolyte is altered with calcium fluoride, aluminum fluoride, and other additives (Peterson & Miller, 2007).

In a typical alumina reduction cell, multiple prebaked carbon anodes are immersed in the electrolyte, and as an intermediate product, oxide ions from alumina dissolution are discharged electrolytically onto the anodes. On the other hand, the oxide intermediate reacts further with the carbon anodes, eventually consuming them by producing gaseous carbon dioxide (CO_2). Inside the electrolyte is a molten aluminum reservoir enclosed in a preformed composite lining and thermally sealed by refractory and insulation components inside a steel shield (Thonstad, 2001). Hence, aluminum is molded by reducing aluminum-containing anions at the electrolyte-metal interface. Although the term cathode is often used to refer to the whole tank of liquid metal and electrolyte, the actual acting cathode is the metal pad or aluminum pool's top surface. The following reaction is the overall reaction of dissolved alumina with carbon to form the products (Barahmand, Jayarathna, et al., 2021d).

$$½\, Al_2O_3\,(dissolved) + ¾\, C\,(s) \rightarrow Al\,(l) + ¾\, CO_2\,(g) \quad (1)$$

This process's total energy conversion is approximately 0.16–0.2 MJ/ton (Barahmand, 2021a). Using titanium diboride cathodes will also substantially reduce energy consumption (up to 20%). The manufacturing of a permanent anode is a more challenging task, and while large-scale experiments are in progress in Japan, Europe, and the United States, no success has been reported. More immediately, sophisticated controls can increase H-H cell efficiency by up to 5%. To anticipate anode effects and optimize its positioning, the pattern of individual cell voltage variations can be monitored and analyzed. Higher energy costs also induce cells to run at lower current densities, resulting in higher efficiency (*Survey of Potential Processes for the Manufacture of Aluminum*, 1979).

The search for feasible alternative processes for aluminum production has been accelerated by rising prices and a lack of large blocks of electrical energy. For instance, the electrolysis of aluminum chloride, sulfide,

nitride; carbothermic reduction of ore or alumina; and the disproportioning reactions of aluminum sulfide or the mono-chloride route can be considered possible alternatives (Barahmand, 2021a). The aluminum industry is undergoing significant changes. It can no longer be selective when it comes to developing sites based on the cost of electricity. Due to the limited electricity available for expansion, the next generation of aluminum smelters must optimize their energy efficiency. This shift has also impacted the importance given to alternative process technology (Grjotheim & Welch, 2016). All of the non-electrolysis processes necessitate extremely high temperatures that can only be reached in an electric furnace. In each case, electrical energy consumption (17.6-22 kWh/kg) is estimated to be higher than that of a Hall-Héroult cell (13.2-17.6 kWh/kg) (*Survey of Potential Processes for the Manufacture of Aluminium*, 1979).

Except for the Alcoa chlorination process, there is no technology for producing aluminum metal that can compete with the Hall-Héroult process in electrical energy consumption. There are some other significant advantages, although, that make the chlorination process attractive. This process does not necessitate the use of pure aluminum oxide as a raw material exclusively. Consequently, the Bayer process could be skipped, eliminating the issue of disposing of vast amounts of red sludge (Barahmand, Jayarathna, et al., 2021a). Carbochlorination can result in relatively high CO_2 concentrations in the process gas, making CO_2 capture and storage easier to implement (Barahmand, 2021a). Carbon's mechanical properties, which are merely a chemical reactant in the chlorination of aluminum chloride, are not required. Consequently, biocarbon may be used instead of coke from petroleum refineries, which the Hall-Héroult process requires, necessitating high mechanical strength and density anodes (Øye, 2019).

The industry has turned its attention to the two-step process of converting alumina to aluminum chloride and then further reducing the aluminum chloride to aluminum metal after failing to find a cost-effective procedure for direct carbothermic reduction of alumina. In the patent literature (Rao & Soleiman, 1986), two chlorination processes are mentioned. The first is a fluidized bed that converts aluminum to aluminum chloride ($AlCl_3$) at a temperature of 590°C. Hydrogen chloride, aluminum hydroxy chloride, aluminum oxychloride, and sodium chloride are also delivered significantly. The sodium comes from the alumina, which contains sodium as an impurity from the Bayer process (Barahmand, 2021a). The stoichiometry of chlorination of gaseous reactants is as follows,

$$Al_2O_3\,(s) + 3Cl_2 + 3CO \rightarrow 2AlCl_3 + 3CO_2 \quad (2)$$

In continuation of the studies on a New Sustainable Aluminum Production (NSAP) process (Barahmand, Aghaabbasi, et al., 2021; Barahmand, Jayarathna, et al., 2021d, 2021a, 2021c, 2021b), this optimization study aims to design an industrial alumina chlorination fluidized bed reactor (isothermally) to achieve the minimum particle outflow and to improve the hydrodynamics inside the reactor by minimizing the channeling effect in the dense phase bed.

2 Overall Design Criteria

The present study aims to design an industrial fluidized bed reactor for pure γ-alumina chlorination in the presence of equimolar carbon monoxide and chlorine gas mixture under the isothermal condition at 700°C. The reactor should be designed for handling 0.6 kg/s of alumina feed. There are no specified limitations for the reactor dimensions or the geometry. However, it is recommended to minimize internals (specifically for cooling and solid circulation). Moreover, because of some technical considerations, such as the possibility of having a considerable percentage of α-alumina in the feed, at the first step, the rector has been designed with no circulation. In the following sections, the main design factors and considerations are discussed.

Circulation System: An early study (Barahmand, Aghaabbasi, et al., 2021) ended up having a turbulent regime using an internal circulation system, but the reactor will be designed for a bubbling regime with better hydrodynamics. On the other hand, considering the highly corrosive environment inside the reactor and the existence of α-alumina impurity in the system, which is not favorable, it avoids circulation internally or externally.

Gas-Solid Separator: The project's primary goal is to minimize the solid escape from the system. Therefore, an external high-efficiency cyclone with an efficiency of 99% will be designed to handle maximum solid carryover. The cyclone is designed for half of the inlet solid flow rate to the reactor (0.01-0.3 kg/s). The other design parameters, such as pressure, fluid properties, and average particle size, will be calculated from simulations.

Regime and Bed Type: As mentioned earlier, the reactor should be designed for the bubbling regime. A free bubbling bed with no internal baffles is recommended to use. To have a smaller bubble size and lower rise velocity, the superficial velocity is chosen in a range close to the minimum bubbling velocity.

Bed Aspect Ratio (H/D): The bed height (H) to the bed diameter (D) ratio is known as the bed aspect ratio (H/D), which is one of the most crucial factors for reactor design calculations (Shaul et al., 2012). The superficial gas velocity by matching the required fluidization regime is used to determine the bed diameter. The bed is generally called tall or deep if the aspect ratio is more significant than unity. On the other side, a shallow bed has an aspect ratio of one or less than one. The precise aspect ratio that marks the transition

between a deep and shallow fluidized bed has yet to be determined (Sathiyamoorthy & Horio, 2003). To have better hydrodynamics in the bed, it has been avoided using a shallow bed. The minimum aspect ratio has been about unity as a safe value (Kunii & Levenspiel, 1991). The given bed aspect ratio selected by the authors in an early study (Barahmand, Jayarathna, et al., 2021a) has been used in the current study.

Reactor Diameter: Based on the carbon monoxide and chlorine mixture's stoichiometry and physical properties, the needed volumetric flow rate of the fluid at the inlet to handle 0.6 kg/s of solid can be calculated easily. On the other hand, the fluid's superficial velocity range is chosen before being very close to minimum bubbling velocity (Regime and Bed Type), which can be calculated too (Barahmand, Aghaabbasi, et al., 2021).

Reactor height: The height of a fluidized bed reactor can be divided into dense and lean phases. Solids lose density as they rise in height. The lean process's height (or freeboard) can be separated into two zones, with the lower section known as the Transport Disengaging Height (TDH). If there is no secondary reaction in the freeboard region, the reactor outlet can be located on top of TDH or above. Otherwise, it can reduce the freeboard and add a more efficient cyclone to the system. Both dense-phase and TDH can be calculated for a bubbling regime (Kunii & Levenspiel, 1991).

Operating Pressure: These parameters highly affect hydrodynamics by influencing fluid's physical properties (Barahmand, Aghaabbasi, et al., 2021). There is no specific pressure in the system because the pressure at the bottom and top of the reactor is not identical, and there is a pressure drop to overcome the bed height of the reactor. The upstream pressure is the bottleneck to define a pressure for the system. It is enough to calculate the needed pressure at the reactor's bottom by choosing a pressure for the fluidized bed outlet. Depending on how the flow boundary at the inlet is defined, this pressure can be calculated automatically by the simulation software (Barracuda®) or defined manually.

Gas Distributor: The distribution mechanism in the gas inlet of the fluidized bed reactor significantly affects hydrodynamics. For example, it can contribute to channeling in the bed or change the bubble size or regime in the bed (Kunii & Levenspiel, 1991). At the first step, a uniform and flat distribution throughout the whole inlet area will be used. In the next step, a grid plate or sparger should be considered a uniform distributing system to be more realistic. Figure 1 shows different types of sparger arrangements in a fluidized bed.

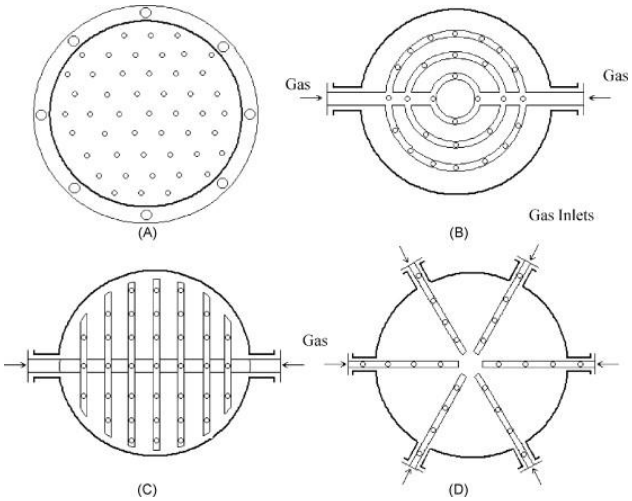

Figure 1. (a) Sieve plate sparger, (b) multiple ring sparger, (c) spider, and (d) pipe sparger (Kulkarni et al., 2009).

Alumina: Many types of alumina have different properties (Barahmand, Jayarathna, et al., 2021d). In the present study, pure γ-alumina has been taken into account, and the effect of impurities is neglected. Each solid particle has many characteristic properties which affect the fluidized bed system. Parameters properties such as particle size distribution, sphericity, voidage, and density should be defined as accurately as possible (Barahmand, Jayarathna, et al., 2021b).

Reactor Geometry: A simple cylindrical reactor with a uniform circular cross-section has been used in early studies (Barahmand, Aghaabbasi, et al., 2021; Barahmand, Jayarathna, et al., 2021a). The reactor's optimum dimensions should be chosen by changing the bed aspect ratio, superficial velocity, and reactor height. An exit geometry should be selected between smooth and abrupt (Harris et al., 2003; Mabrouk et al., 2008). Any change in the reactor geometry can be applied to achieve lower particle escape and desirable hydrodynamics. For example, cylindrical FB reactors inherited several weak points. Yang et al. have investigated the effect of the expanded cross-section at the top of the reactor and related hydrodynamics.

Reaction kinetics: The present study simulates the single overall reaction (2) in Barracuda®. The reaction kinetics are based on (Barahmand, Jayarathna, et al., 2021d). Although the alumina chlorination at 700℃ is very fast and the reactor height can be reduced, the hydrodynamics inside the reactor plays a crucial role. The H/D highly affects the overall reactor height, and the reported value is minimum equal to unity (Kunii & Levenspiel, 1991) for Geldart A particles. On the other hand, reaction kinetics is highly correlated with temperature, particle size distribution, and porosity (Barahmand et al., 2021d).

Heat Transfer: Although the primary goal of the present study is to touch the project objectives under isothermal conditions at 700℃, the thermal study of the chlorination process is one of the most critical design considerations (Barahmand et al., 2021c). The literature confirms that the best and optimum temperature for the alumina chlorination process is 700℃, but taking the industrial design limitations into account, 600℃ will be the optimum temperature (Gokcen, 1983).

Solid Feeder: The current fluidized bed is a continuous reactor that alumina is fed to the reactor with a feeding rate of 0.6 kg/s. In general, the powder can be transported mechanically or pneumatically (or air-assisted). The screw feeder, as an example of a mechanical conveyor or pneumatic conveying system, can be used in the design. In this project, it is considered that the powder is injected pneumatically using CO_2. Another critical point is the location and direction of the injection. In some cases, particles' downward movement positively affects the reaction (For example, alumina chlorination in fluidized bed (Gokcen, 1983)). However, taking the other considerations, such as possible particle outflow, into account, placing the particle injection at the reactor's bottom side-wall is beneficial.

Construction Material: Although the current study does not directly deal with the materials, reactor design is affected by general considerations. The typical fluidized bed uses a carbon steel shell lined with a particular alumina refractory (Barahmand, Aghaabbasi, et al., 2021).

Erosion: There are three primary sources for erosion in a fluidized bed, temperature, chemicals, and solid particles (Barahmand, 2021b). All the internal surfaces that contact a corrosive or very high-temperature fluid are in danger of erosion. On the other hand, in higher velocities, solid particles can cause erosion, and usually, it is associated with transitional and directional changes in the system. For example, most erosive wear may occur in the internal cyclone wall or near the elbow of bent pipes. In the present study, a particular alumina refractory is considered a reactor lining to protect against very high temperatures and chemical corrosion. Although alumina particles are highly abrasive (Haugland et al., 2019), this effect may be minimal because of the low superficial velocity in the system. The erosion has not been considered in this study.

Drag Model: The force acting on a particle by the fluid flow around it is determined by the particle's drag model. The Barracuda® provides a range of predefined drag models that the WenYu-Ergun blended drag model could be more suitable for the current study. Since the Wen and Yu correlation is appropriate for more dilute systems and the Ergun relationship is appropriate at higher packing fractions, proposed a drag function blending both the Wen-Yu and Ergun functions as the following (Gidaspow, 2012).

For $\theta_p < 0.75\theta_{cp}$, the drag model can be calculated by the Wen-Yu model (D_1).

$$D_1 = \begin{cases} \frac{24}{Re}\theta_f{}^{-2.65} & Re < 0.5 \\ \frac{24}{Re}\theta_f{}^{-2.65}(1 + 0.15Re^{0.687}) & 0.5 \le Re \le 1000 \\ 0.44\theta_f{}^{-2.65} & Re > 1000 \end{cases} \quad (3)$$

For $\theta_p > 0.85\theta_{cp}$, the drag model can be calculated by the Ergun drag function (D_2) as below.

$$D_2 = 0.5\left(\frac{180\theta_p}{\theta_f Re} + 2\right)\frac{\rho_f|u_f - u_p|}{r_p\rho_p} \quad (4)$$

For $0.75\theta_{cp} \le \theta_p \le 0.85\theta_c$, the following equation can derive the drag model:

$$D = (D_2 - D_1)\left(\frac{\theta_p - 0.75\theta_{cp}}{0.85\theta_{cp} - 0.75\theta_{cp}}\right) \quad (5)$$

Where θ_p and θ_f are the particle and fluid volume fraction respectively, θ_{cp} is the particle volume fraction at the close pack[1], Re is the Reynolds number, u_f and u_p are fluid and particle velocity, ρ_p is particle density and r_p is the average particle radius.

3 3D Multiphase Particle-in-Cell Approach

Barracuda®'s technology is based on 3D Multiphase Particle-in-Cell (3D-MP-PIC), a patented computational technique for CFD simulation of gas-particle flows that includes close fluid-particle coupling as well as careful consideration of thermal physics and reaction chemistry (Ahmadpour Samani et al., 2020). For dense particle flows, a three-dimensional, multiphase particle-in-cell approach is presented. The computational technique uses a continuum model to solve the governing equations of the fluid phase and a Lagrangian model to solve the governing equations of the particle phase (Snider, 2001). Through mapping particle properties to an Eulerian grid and then mapping back-calculated stress tensors to particle positions, the difficulties associated with estimating inter-particle interactions with dense particle flows with volume fractions above 5% have been removed. A robust sub-grid particle normal stress model for isolated particles that eliminates the need for an implicit measurement of normal particle stress on the grid has been presented. The properties of interpolation operators that provide compact support, conservatism, and a quick solution for

[1] The close pack volume fraction specifies the maximum volume fraction of particles when they are packed randomly.

a broad particle population are defined. The solution scheme allows for particle forms, sizes, and mass distributions with no numerical diffusion from the Lagrangian particle equations. The fluid momentum and pressure equations are indirectly solved, resulting in a stable solution.

There are two approaches to this, the Continuum and the Particulate Phase. The continuity equation for a fluid with no interphase mass transfer is (Verma & Padding, 2020).

$$\frac{\partial \theta_f}{\partial t} + \nabla.\left(\theta_f u_f\right) = 0 \tag{6}$$

The momentum equation for the fluid will be as (7).

$$\frac{\partial\left(\theta_f u_f\right)}{\partial t} + \nabla.\left(\theta_f u_f u_f\right) = -\frac{1}{\rho_f}\nabla P - \frac{1}{\rho_f}\mathrm{F} + \mathrm{g}\theta_f \tag{7}$$

where, g is the acceleration gravity, F is "the rate of momentum exchange per volume between the fluid and particle phases," P is fluid pressure, and ρ_f is the fluid density. In the Particulate Phase, the particle probability distribution function $\emptyset\,(X, u_p, \rho_p, \Omega_p, t)$ is used to define the dynamics of the particle process, where X is the particle position, u_p is the particle velocity, ρ_p is the particle density, and Ω_p is the particle volume (Snider, 2001). For the time being, it is thought that each particle's mass remains stable over time (i.e., no mass transfer between particles or to the fluid), although particles may vary in size and density. The time evolution is obtained by solving a Liouville equation (Williams, 1985) for the particle distribution function.

$$\frac{\partial \emptyset}{\partial t} + \nabla.\left(\emptyset\, u_p\right) + \nabla_{u_p}.(\emptyset A) = 0 \tag{8}$$

where ∇_u is the divergence operator concerning velocity. Using the definition from (Andrews & O'Rourke, 1996), the discrete particle acceleration, A, can be defined as,

$$A = D_p\left(u_f - u_p\right) - \left(\frac{1}{\rho_p}\nabla P + \frac{1}{\theta_p \rho_p}\tau\right) + \mathrm{g} \tag{9}$$

where, the terms describe acceleration due to aerodynamic drag, pressure gradient, interparticle stress gradient, and gravity, respectively, the Gidaspow drag model (Gidaspow, 2012), which is a combination of the Wen and Yu (Wen & Yu, 1966) and the Ergun (Ergun, 1952) drag models (3-5), can be used in (9). The present study optimizes the alumina chlorination in a fluidized bed reaction having a bubbling regime. The superficial velocity of the fluid is close to the minimum bubbling velocity.

4 CPFD Simulations

The standard range for the bed aspect ratio (H/D) is not thoroughly investigated and discussed in the literature. The best aspect ratio used in the present study is based on the authors' previous work (Barahmand et al., 2021a), equal to 2. The reaction kinetics and alumina properties are explained elsewhere (Barahmand et al., 2021d). The base model was developed with simple cylindrical geometry and a smooth exit in the first step. The smooth exit does not affect the hydrodynamics of the reactor top (Mabrouk et al., 2008).

4.1 Base Model

The chlorine concentration (as a factor of conversion rate) and particle distribution (as a factor of reactor hydrodynamics) have been studied in the model. In the first step, the gas reactants are distributed homogeneously from the bottom of the reactor (ideal distribution). Figure 3 illustrates the particle mass flux in different heights in the reactor. As seen in the figure, the red ring emphasizes particle escape through the reactor wall.

Studying the particle outflow shows that for uniform inflow, the average particle outflow at the pseudo-steady-state is about 0.38 kg/s, almost 63% of the particle inflow (Figure 2). On the other hand, the particle escape through the wall harms reaction conversion. 'Due to high resistance within the particle bed, the fluid temps to escape close to the reactor wall, increasing fluid velocity in the near-wall region. As a result, the reactants have less time to react.

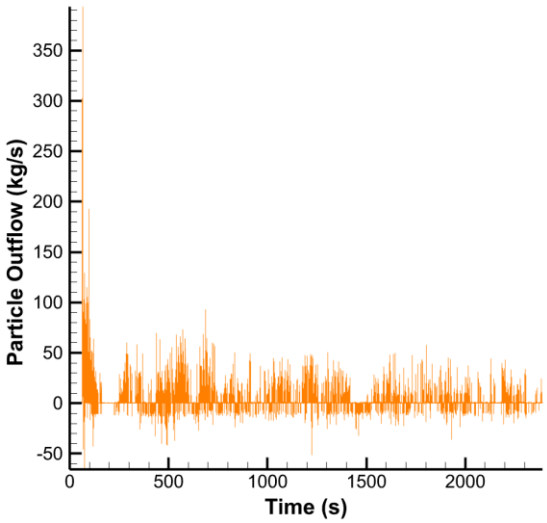

Figure 2. Particle outflow (kg/s) with uniform distribution

A non-uniform distribution pattern (Figure 4) with higher velocity in the middle and gradually decreasing toward the inner walls (Figure 5) has been applied to the system to solve this problem. The results have shown a significant change in the reactor hydrodynamics and particle escape.

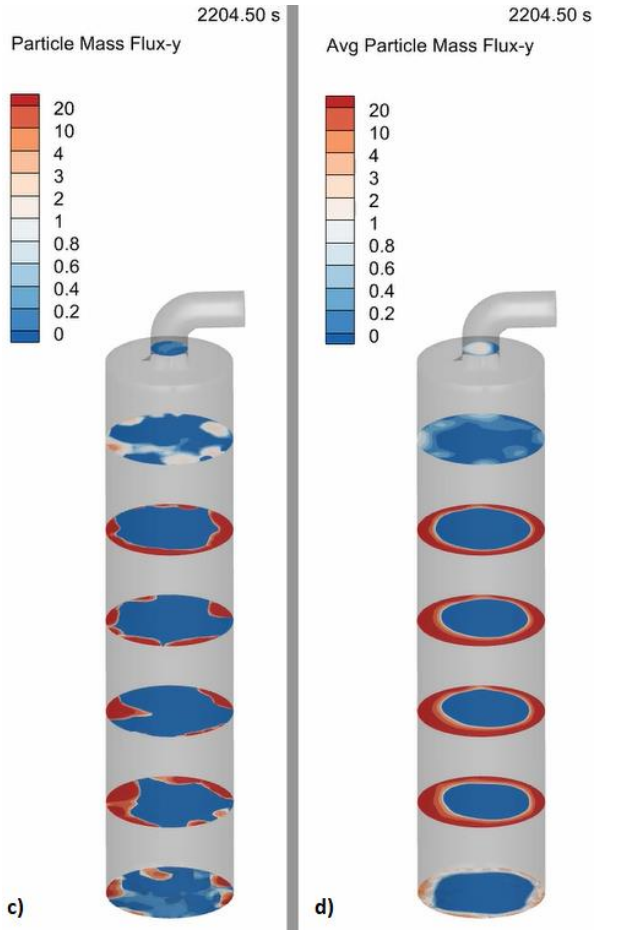

Figure 3. The particle mass flux (kg/sm^2) in different heights with a uniform distribution. c) Particle mass flux at the specific time, and d) Average particle mass flux in the last 300 seconds.

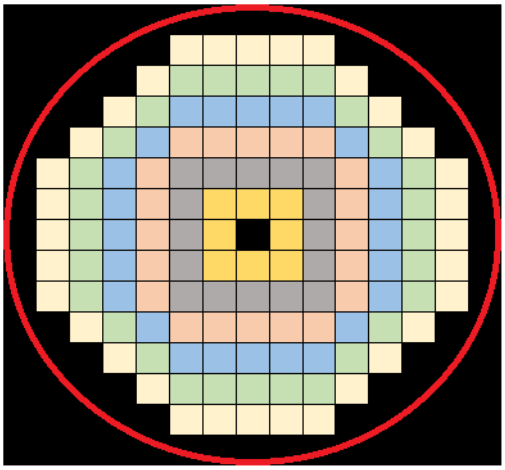

Figure 4. Defined non-uniform ring distribution in Barracuda®

Changing the fluid distribution pattern shows a considerable change in the bed's hydrodynamics. As seen in Figure 6, the ring area is turned to a crescent shape. Compared with uniform distribution, the particle outflow is 0.59 kg/s which is two times more and almost identical to the particle feed rate.

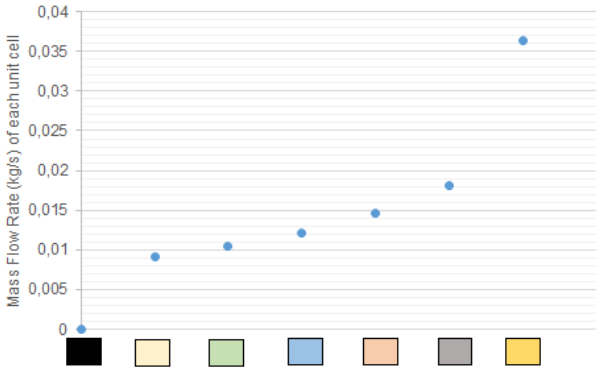

Figure 5. Inlet gas ($CO+Cl_2$) mass flow rate of each cell-color scale refers to Figure 4.

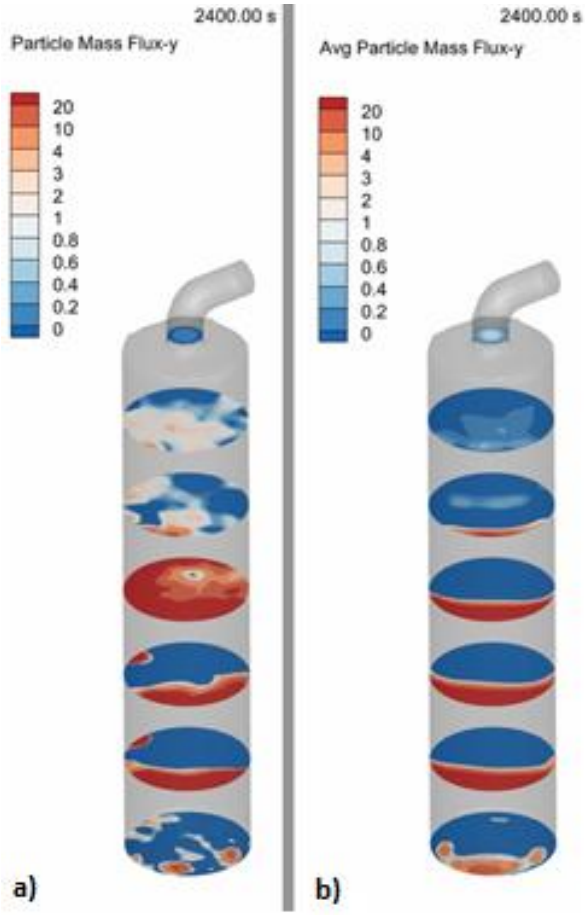

Figure 6. The particle mass flux (kg/s.m^2) in different heights with the non-uniform distribution. a) Particle mass flux at the specific time, and b) Average particle mass flux in the last 300 seconds.

Although the hydrodynamics has experienced a considerable change, the chlorine concentration through the reactor is almost constant due to the very high reaction rate. Table 1 gives the chlorine concentration through the reactor from bottom to top in the specified heights in Figure 3 and Figure 6. Although the results confirm that the conversion rate becomes complete at the bottom of the reactor, reducing the reactor height is

not suggested to keep the best hydrodynamics (Barahmand, 2021a).

Table 1. Average Cl_2 concentration (mg/l) in different heights of the reactor.

Level	**Uniform**	**Non-Uniform**
0	289.27	65.23
1	0.35	0.59
2	0.05	0.04
3	0.03	0.02
4	0.02	0.02
5	0.02	0.04
6	0.03	0.03
7	0.02	0.03

In these simulations, the particle escape from the top of the reactor is the biggest challenge.

4.2 Optimized model

As discussed in Section 2, Yang et al. have used an expanded section to reduce the slugging and to solve this problem effectively. Therefore, it may positively affect reducing particle outflow (Yang & Keairns, 1980). Figure 7 illustrates a schematic view of the new geometry with the expanded cross-sectional at the top. In the current simulation, a total number of 65000 cells have been used.

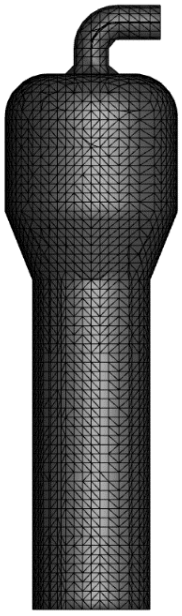

Figure 7. The meshed geometry with the expanded cross-sectional area on top

Similarly, for uniform and non-uniform distributions, the bed hydrodynamics, particle outflow, and Cl_2 concentration have been studied. As expected, the geometry shows no effect on the reaction and chlorine consumption.

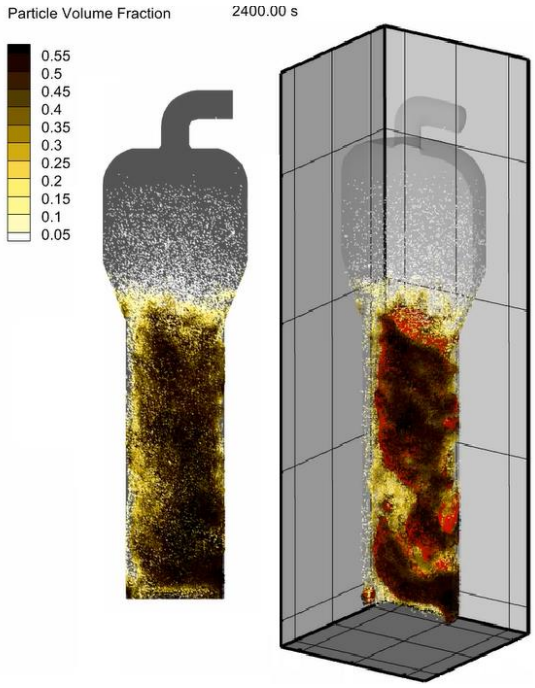

Figure 8. Particle distribution through the reactor with the non-uniform flow.

As seen in Figure 8, the expanded bed is located in the bottom cylindrical section of the reactor. As a result, a negligible effect on particle escape through the reactor wall has been expected. In comparison with cylindrical models, Figure 9 and Figure 10 confirm this phenomenon.

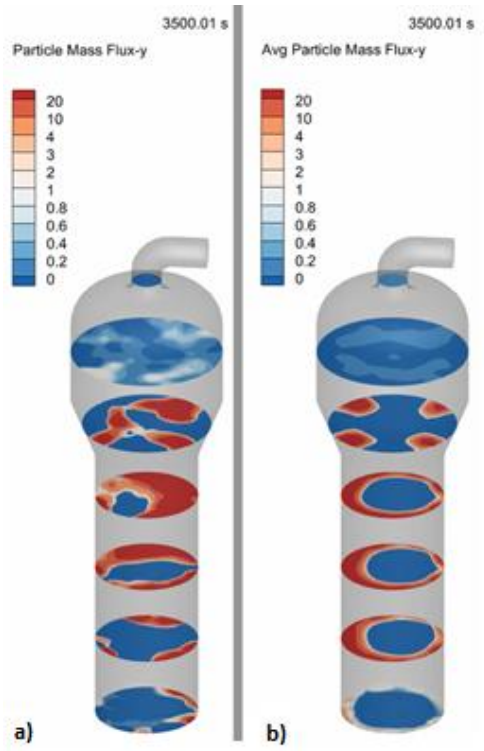

Figure 9. The particle mass flux (kg/s.m^2) in different heights with a uniform distribution. a) Particle mass flux at

the specific time, and b) Average particle mass flux in the last 300 seconds.

Nevertheless, in both cases, particle outflow has been dropped significantly. Table 2 gives comparative data for all cases.

Table 2. Particle outflow (kg/s) in different cases

	Uniform gas Distribution	Non-Uniform gas Distribution
Cylindrical	0.38	0.59
New Design	0.15	0.0004

Although the optimized geometry has shown a remarkable performance in reducing the particle escape from the top of the reactor, this design may suffer from the possibility of particle deposition and caking phenomenon in the conical top sections. Applying a non-uniform inlet flow pattern has reduced the channeling effect, and has resulted less scape through the sidewall has been observed. Figure 11 shows a channel created inside the bed.

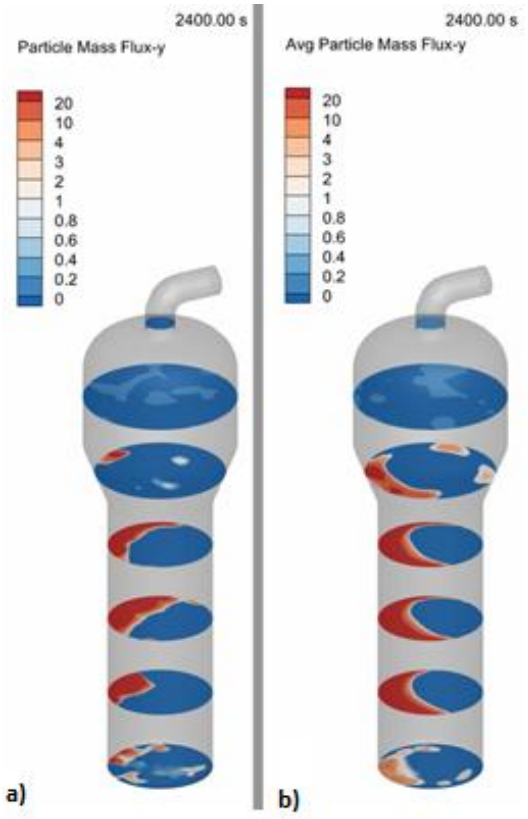

Figure 10. The particle mass flux (kg/s.m^2) in different heights with the non-uniform distribution. a) Particle mass flux at the specific time, and b) Average particle mass flux in the last 300 seconds.

5 Conclusion

The modified geometry leads to minimizing the particle outflow significantly and helps the reactor's hydrodynamics. On the other hand, in contrast with simple cylindrical geometry, non-uniform gas distribution contributes to reducing high gas escape close to the wall, enhancing the reaction. Combining geometrical modification and change in gas injection, the reactor has now shown quite promising performances. It is crucial to validate the CFD simulation data with a lab-scale experimental unit as future work. Moreover, even though current simulations are done based on mess specifications from CPFD software (Barracuda®), the mesh convergence can be helpful to find the right mesh size and further improvement of the model.

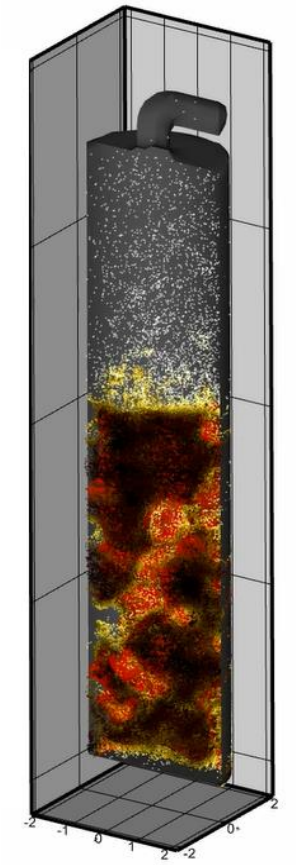

Figure 11. Channeling effect in a cylindrical reactor with uniform distribution.

References

N. Ahmadpour Samani, C. Jayarathna, and L. A. Tokheim. CPFD simulation of enhanced cement raw meal fluidization through mixing with coarse, inert particles. *In proceedings - 61st SIMS Conference on Simulation and Modelling SIMS 2020*, Finland, 2020. doi:10.3384/ecp20176399

M. J. Andrews and P. J. O'Rourke. The multiphase particle-in-cell (MP-PIC) method for dense particulate flows. *International Journal of Multiphase Flow*, *22*(2), 379–402. 1996. doi:10.1016/0301-9322(95)00072-0

Z. Barahmand. *Design of an Industrial Chlorination Reactor using CPFD Simulations*, Master's Thesis. University of South-Eastern Norway, 2021a.

Z. Barahmand, O. Aghaabbasi, E. K. L. Rustad, J. L. Salcido, C. Jayarathna, and C. Ratnayake. Designing of a medium-scale circulating fluidized bed reactor for chlorination of processed aluminum oxide. *In proceedings - 1st SIMS EUROSIM Conference on Modelling and Simulation*, Finland, 2021.

Z. Barahmand, C. Jayarathna, and C. Ratnayake. CPFD modeling of the hydrodynamics and reaction kinetics of alumina chlorination in an industrial fluidized bed reactor. *In proceedings - 1st SIMS EUROSIM Conference on Modelling and Simulation*, Finland, 2021a.

Z. Barahmand, C. Jayarathna, and C. Ratnayake. Sensitivity and uncertainty analysis in a fluidized bed reactor modeling. *In proceedings - 1st SIMS EUROSIM Conference on Modelling and Simulation*, Finland, 2021b.

Z. Barahmand, C. Jayarathna, and C. Ratnayake. Study of the thermal performance of an industrial alumina chlorination reactor using CPFD simulation. *In proceedings - 1st SIMS EUROSIM Conference on Modelling and Simulation*, Finland, 2021c.

Z. Barahmand, C. Jayarathna, and C. Ratnayake. The effect of alumina impurities on chlorination in a fluidized bed reactor: A CPFD study. *In proceedings - 1st SIMS EUROSIM Conference on Modelling and Simulation*, Finland, 2021d.

D. Donaldson and B. Raahauge. *Essential Readings in Light Metals, Alumina and Bauxite*. John Wiley & Sons, 2013.

S. Ergun. Fluid flow through packed columns. *Fluid Flow Through Packed Columns*, *48*, 89–94. Scopus, 1952.

D. Gidaspow. *Multiphase Flow and Fluidization: Continuum and Kinetic Theory Descriptions, 2012*.

N. A. Gokcen. *Rates of chlorination of aluminous resource*, pages 28, U.S. Department of the Interior, Bureau of Mines, 1983.

K. Grjotheim and B. Welch. Impact of Alternative Processes for Aluminium Production on Energy Requirements. In G. Bearne, M. Dupuis, & G. Tarcy (Eds.), *Essential Readings in Light Metals: Volume 2 Aluminum Reduction Technology*, pages 1049–1055. Springer International Publishing, 2016. doi:10.1007/978-3-319-48156-2_154

A. T. Harris, J. F. Davidson, and R. B. Thorpe. Influence of exit geometry in circulating fluidized-bed risers. *AIChE Journal*, *49*(1), 52–64, 2003. doi:10.1002/aic.690490107

I. B. Haugland, O. Kjos, A. Røyset, P. E. Vullum, T. A. Aarhaug, and M. Halstensen. Alumina Scale Composition and Growth Rate in Distribution Pipes. In C. Chesonis (Ed.), *Light Metals 2019* (pp. 697–706). Springer International Publishing, 2019. doi:10.1007/978-3-030-05864-7_86

A. V. Kulkarni, S. V. Badgandi, and J. B. Joshi. Design of ring and spider type spargers for bubble column reactor: Experimental measurements and CFD simulation of flow and weeping. *Chemical Engineering Research and Design*, *87*(12), 1612–1630, 2009. doi:10.1016/j.cherd.2009.06.003

D. Kunii and O. Levenspiel. *Fluidization Engineering*. Butterworth-Heinemann, 1991.

R. Mabrouk, J. Chaouki, and C. Guy. Exit effect on the hydrodynamics of the internal circulating fluidized bed riser. *Powder Technology - POWDER TECHNOL*, *182*, 406–414, 2008. doi:10.1016/j.powtec.2007.07.008

B. Øye. Could the chloride process replace the Hall-Héroult process in aluminum production?. 2019, March 28.

W. S. Peterson and R. E. Miller. *Hall-Héroult Centennial: First Century of Aluminum Process Technology*, 2007.

S. Prasad. Studies on the Hall-Héroult aluminum electro winning process. *Journal of the Brazilian Chemical Society*, *11*, 245–251, 2000. doi:10.1590/S0103-50532000000300008

Y. K. Rao and M. K. Soleiman. *Alumina chlorination*. United States Patent No. US4565674A, 1986. https://patents.google.com/patent/US4565674A/en

D. Sathiyamoorthy and M. Horio. On the influence of aspect ratio and distributor in gas fluidized beds. *Chemical Engineering Journal*, *93*(2), 151–161, 2003. doi:10.1016/S1385-8947(02)00257-7

S. Shaul, E. Rabinovich, and H. Kalman. Generalized flow regime diagram of fluidized beds based on the height to bed diameter ratio. *Powder Technology*, *228*, 264–271, 2012. doi:10.1016/j.powtec.2012.05.029

D. M. Snider. An Incompressible Three-Dimensional Multiphase Particle-in-Cell Model for Dense Particle Flows. *Journal of Computational Physics*, *170*(2), 523–549, 2001. doi:10.1006/jcph.2001.6747

Survey of potential processes for the manufacture of aluminium (ANL/OEPM-79-4). Little (Arthur D.), Inc., Cambridge, MA (USA), 1979. doi:10.2172/5669730

J. Thonstad, J. Aluminium electrolysis: Fundamentals of the Hall-Héroult process, 2001.

V. Verma and J. T. Padding. A novel approach to MP-PIC: Continuum particle model for dense particle flows in fluidized beds. *Chemical Engineering Science: X*, *6*, 100053, 2020. doi:10.1016/j.cesx.2019.100053

C. Wen and Y. Yu. Mechanics of fluidization. *The Chemical Engineering Progress Symposium Series*, *62*, 100–111, 1966.

F. A. William. *Combustion Theory*. The Benjamin/Cummings Publishing Company, Inc, 1985.

W. Yang and D. Keairns. *The effect of an expanded section on slugging*, 1980. doi:10.1002/AIC.690260124